Temperatures of the A.D. 79 pyroclastic density current deposits (Vesuvius, Italy)

R. Cioni
Dipartimento di Scienze della Terra, Cagliari, Italy

L. Gurioli
Istituto di Geoscienze e Georisorse, Consiglio Nazionale delle Ricerche, Pisa, Italy

R. Lanza and E. Zanella
Dipartimento di Scienze della Terra, Torino, Italy

Received 18 October 2002; revised 26 August 2003; accepted 20 October 2003; published 18 February 2004.

[1] The temperature of the deposits left by different types of pyroclastic density currents (PDCs) of the A.D. 79 "Pompei" eruption of Vesuvius was estimated by measuring the thermal remanent magnetization (TRM) of lithic clasts carried by the currents. More than 200 lava clasts and roof tile fragments were collected at different sites and distances from the vent. The estimated temperatures fall in the range 180–380°C, although most of the samples show temperatures (T) in the range 240–340°C. This interval occurs for both the deposits of the same eruptive unit sampled at different sites and those derived from PDCs with similar physical characteristics. The sedimentological features coupled with the TRM data allow us to highlight the main processes controlling the T variability of the deposits and of their emplacing currents. The results reveal that air ingestion, involvement of external water, as well as transport and emplacement processes of the PDC are the most important factors in decreasing the emplacement T. The amount of lithic clasts carried by the currents does not play an important role in changing the final temperature because of the grain size and initial high T of these fragments. *INDEX TERMS:* 1527 Geomagnetism and Paleomagnetism: Paleomagnetism applied to geologic processes; 8404 Volcanology: Ash deposits; 8414 Volcanology: Eruption mechanisms; *KEYWORDS:* temperature, A.D. 79, pyroclastic density currents, deposits, Vesuvius

Citation: Cioni, R., L. Gurioli, R. Lanza, and E. Zanella (2004), Temperatures of the A.D. 79 pyroclastic density current deposits (Vesuvius, Italy), *J. Geophys. Res.*, *109*, B02207, doi:10.1029/2002JB002251.

1. Introduction

[2] The emplacement temperature of pyroclastic density current (PDC) deposits is a function of the initial temperature of the PDC, the size and provenance of its constituents, the extent of cooling during transport, and the rate of sedimentation. Estimation of emplacement temperature has long been addressed by measuring the thermal remanent magnetization (TRM) of both lithic and pumice fragments in pyroclastic deposits. This technique was developed by *Aramaki and Akimoto* [1957] and successfully applied in several cases around the world [*Wright*, 1978; *Hoblitt and Kellogg*, 1979; *Kent et al.*, 1981; *McClelland and Druitt*, 1989; *Clement et al.*, 1993; *Downey and Tarling*, 1991; *McClelland and Thomas*, 1993; *Mandeville et al.*, 1994; *Bardot*, 2000].

[3] As a general model, when a lithic clast is first incorporated into a PDC, it is heated to a temperature close to the mean temperature of the flow, and the portion of its magnetic remanence carried by ferromagnetic grains with blocking temperatures (T_b) lower than the PDC temperature is erased. During cooling after deposition a new, low-T_b magnetization is acquired, coherently oriented along the Earth's magnetic field at the time of eruption. The lithic clasts in these deposits thus have a two-component magnetization: a randomly oriented high-T_b component and a uniformly oriented low-T_b component. Progressive thermal demagnetization enables us to isolate the two components. The emplacement temperature can thus be determined as the upper limit of the low-T_b component of the TRM [*Bardot*, 2000]. This model is actually oversimplified. Considering the time the different constituents of a PDC need to reach thermal equilibrium, it is more appropriate to interpret the results of the TRM analysis as the temperature reached by the whole deposit after coming to rest and before extensive cooling began [*Bardot and McClelland*, 2000]. This temperature does not necessarily coincide with the emplacement temperature of the PDC. For this reason we will discuss the results of our TRM measurements in terms of the temperature of the deposit as a whole (T_{dep}) instead of an emplacement temperature.

0148-0227/04/2002JB002251$09.00

[4] Notwithstanding the extensive use of TRM measurements in the study of volcanic rocks, there are only a few cases [*McClelland and Thomas*, 1993] where they have been used to develop a detailed picture of the depositional history of the entire pyroclastic sequence from a single eruption. In a pioneering work, *Kent et al.* [1981] estimated paleomagnetic temperatures of 10 samples collected from some flow units of the A.D. 79 Vesuvius eruption that crop out inside the archaeological excavations at Ercolano. In this paper, we discuss the results of TRM measurements on samples from the whole spectrum of different PDC deposits of the A.D. 79 eruption. Previous sedimentological studies [*Cioni et al.*, 1992b; *Gurioli et al.*, 1999; *Gurioli*, 2000] allow us to interpret these deposits in terms of transport and depositional mechanisms and to quantify some of the main physical parameters of the related PDCs.

[5] For this study TRM was measured on both lithic fragments and Roman tiles embedded in the deposits. These tiles, picked up at ambient temperature by the flowing PDCs and promptly deposited down flow, clearly record the temperature reached by the whole deposit after deposition rather than the temperature reached inside the flowing PDC. Samples were collected from different flow units as well as from different parts of the same flow unit (Figure 1a). The results allow us to infer the temperature dependence of the following three parameters: (1) eruptive processes (magmatic versus phreatomagmatic; PDC generation from the total collapse or marginal instability of the convective column), (2) transport and depositional processes (dilute versus concentrated currents; supercritical flow; travel distance), and (3) the composition of the deposits (differences in grain-size distribution and lithic content).

2. Sedimentological Features of the A.D. 79 PDC Deposits

[6] On 24 August A.D. 79, Vesuvius erupted violently, ejecting huge amounts of pumice and ash. These were both deposited over distances of thousands of kilometers as air fall from the Plinian column and around the volcano from PDCs. It was these PDCs that ravaged and buried several Roman towns (Figure 1a). The eruption progressed from a weak phreatomagmatic opening phase to a climactic Plinian phase and finally to a phreatomagmatic phase triggered by the collapse of the caldera [*Cioni et al.*, 1999] (Figure 1a). Most of the erupted magma was dispersed as fallout pyroclastics from a strongly convective column during the Plinian phase. The fallout phase lasted about 20 hours [*Sigurdsson et al.*, 1982], depositing phonolitic "white" pumice (EU2f) followed by phonotephritic "gray" pumice (EU3f). During the Plinian phase, some PDCs were generated by the discontinuous collapse of marginal portions of the convective column (EU3pfi). These episodes are recorded by thinly stratified ash layers, that grade locally into thick, massive, pumice-rich flow deposits. The fallout phase was closed by total column collapse that generated a radially dispersed PDC (EU3pf). The magmatic phase stopped with the emplacement of lithic-rich deposits toward the N and NW (EU3pfL, in Figure 1a) during collapse of the shallow magma reservoir.

[7] The final (phreatomagmatic) phase (EU4 to EU8) is recorded by the deposits of several PDCs. The onset of this phase was characterized by the restoration of a short-lived, convective Plinian column [*Cioni et al.*, 1996] which rapidly collapsed, generating a highly energetic, radially dispersed, turbulent PDC (EU4). This was followed by several PDCs, which locally deposited stratified-to-massive beds along the main valleys of the volcano (EU5). The paroxysmal phase of caldera collapse is marked by very coarse, lithic-rich breccia flow deposits (EU6). After the emplacement of a second, widespread, turbulent PDC (EU7), the waning stages of the eruption emplaced several lithic-rich PDCs, whose deposits are well exposed in the northern sector (EU8L, Figure 1a), and a thick, widely dispersed, phreatomagmatic accretionary lapilli-bearing ash (EU8). Grain size, composition, and morphological features of the juvenile fragments all suggest a progressive shift from "dry" to "wet" depositional conditions during the phreatomagmatic phase of the eruption, as suggested by *Barberi et al.* [1989] and *Cioni et al.* [1992a].

[8] The A.D. 79 PDC deposits vary from stratified to massive, showing large facies variations both within individual flow units and between different flow units. The sedimentological features suggest a complete gradation from dilute, fully turbulent currents to dense, non turbulent flows [*Druitt*, 1998; *Freundt and Bursik*, 1998; *Burgisser and Bergantz*, 2002]. At least four main types of PDC deposits may be recognized in the A.D. 79 succession, and related to transport and depositional features of the emplacing currents (Table 1 and Figures 1b, 1c, 1d, and 1e) [*Gurioli et al.*, 1999; *Gurioli*, 2000; *Gurioli et al.*, 2002]. These are type 1, thin, fine-grained, cross-stratified deposits, emplaced through progressive aggradation from dilute, fully turbulent currents of small volume (EU2/3pf and EU3pfi); type 2, thick, fining upward, massive to stratified deposits, emplaced by progressive aggradation from a sustained, decelerating, turbulent, stratified currents (EU4 and EU7); type 3, thick, stratified deposits, laterally and vertically grading into massive deposits, emplaced by progressive aggradation from a sustained current characterized by a depositional boundary layer in which rapid transition from turbulent to nonturbulent deposition occurred locally (EU3pf); and type 4, very thick, massive, valley-ponded deposits emplaced "en masse" from dense, nonturbulent, low-velocity flows (EU3pfL, EU6, and EU8L).

3. Methods

[9] In order to detect possible variations in the temperature of the deposits several lithic fragments were collected from the main PDC units at different sites and distances from the vent. TRM analyses were made on lithic fragments (lavas and minor cumulates) and chips of roof tiles from Roman buildings destroyed by the flows. Pumice lumps were avoided because of their generally weaker magnetization than lithic clasts, as discussed by *McClelland and Thomas* [1993].

3.1. Sampling

[10] PDC deposits of the A.D. 79 eruption were sampled at 13 sites around Vesuvius (Figure 1a). The deposits related to the Plinian fallout phase were not sampled. Samples of the deposits relating to the magmatic (EU2/3pf, EU3pfi, and EU3pf) and phreatomagmatic phases (EU4, EU6 and EU7)

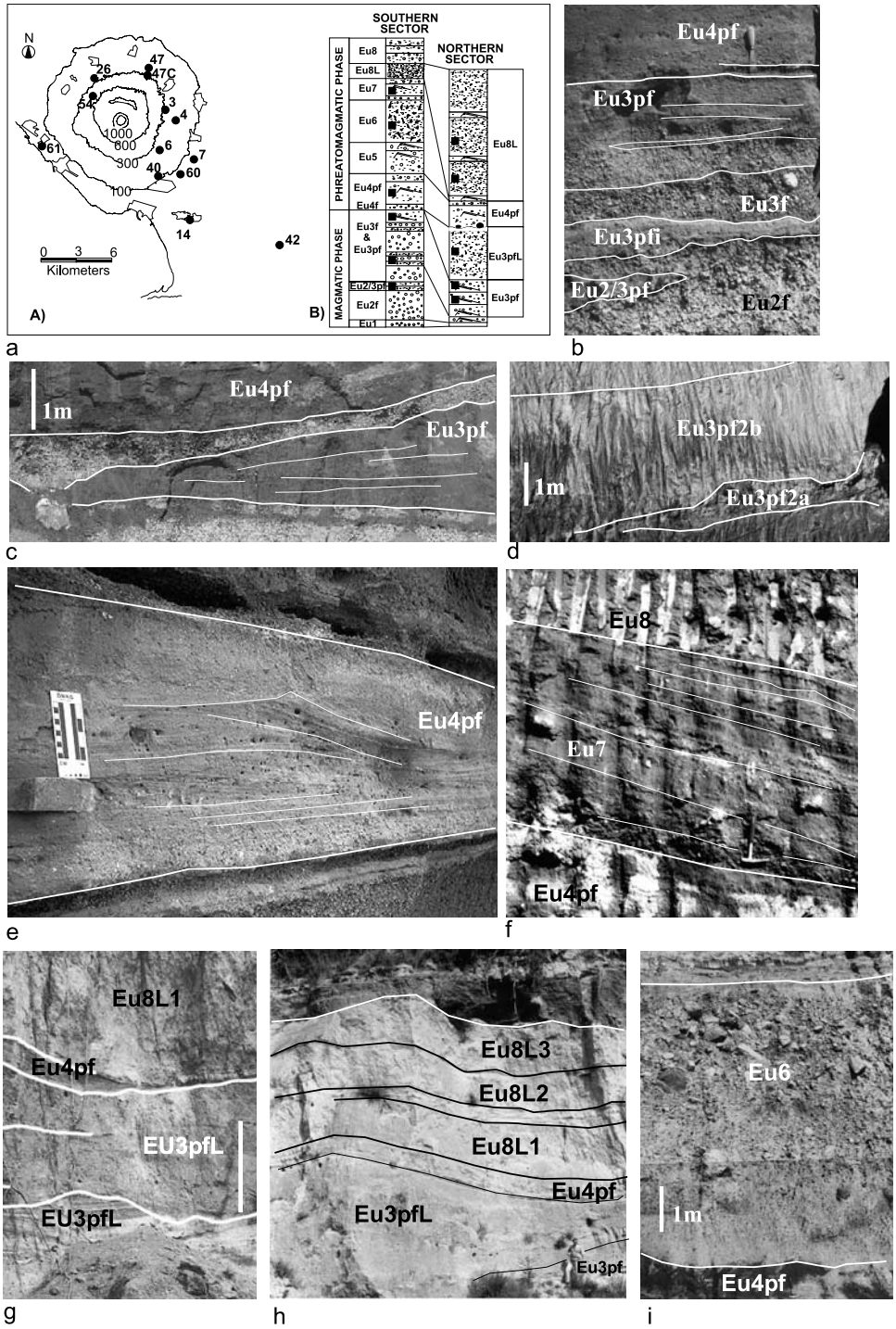

Figure 1. (a) Map of Vesuvian region. Dots indicate studied sections. Site toponymy is given in Table 2. Schematic stratigraphy of the deposits of the 79 A.D. eruption is shown. Squares indicate position of the collected samples; (b) type 1, thin, fine-grained, cross-stratified PDC deposits (EU2/3pf and EU3pfi), followed by type 3, stratified deposit (EU3pf), Terzigno; (c) type 3, thick, stratified deposits laterally and vertically grading into massive PDC deposits (EU3pf), close to Cava Molara; (d) type 3, thick massive facies (EU3pf2b) and fines-poor ground layer (EU3pf2a), Ercolano; (e) type 2, thick, fining upward massive to stratified PDC deposits (EU4), Pompei; (f) type 2, thick, fining upward massive to stratified PDC deposits (EU7), Cinque Vie; (g and h) type 4, thick, massive, PDC deposits (EU3pfL and EU8L), Pollena; (i) type 4, very thick, massive, valley-pounded, coarse-grained, lithic-rich deposit (EU6), close to Cava Molara.

Table 1. Classification of the PDC Deposits of the A.D. 79 Eruption[a]

Eruption Unit	Description of the Deposits	Mechanism of Transport and Deposition	Dispersal and Maximum Runout	Mean Grain Size Mdϕ	Lithic Content and Lithology
			Type 1		
EU2/3pf EU3pfi	Thin, plane parallel to cross-bedded deposits, locally thickening in correspondence to topographic depressions where they still maintain a thinly stratified aspect. Fine-grained deposits with lithic lapilli scattered in pumice rich layers	Deposition through progressive aggradation from dilute, turbulent currents of small volume	Mainly dispersed around the eruptive center. Maximum runout up to 9 km (in the southern sector)	EU2/3pf: 0; 4 EU3pfi: −2; 2	EU2/3pf: 20% EU3pfi: 10% Fresh leucite-bearing lavas and minor limestones and marbles
			Type 2		
EU4 EU7	Stratified, undulatory bedded to dune bedded deposits in very proximal sites (thickness up to 4 m), to massive and laminated beds at about 6–7 km from the vent to massive, accretionary lapilli-bearing beds at distal reaches. They are capped by an up to 20 cm thick accretionary lapilli- bearing ash layer. The deposits are formed by pumice and lithic lapilli set in a polymodal matrix of fine and coarse ash. Blocks are subordinate and related to ballistic fall-out. The deposits are always fining upward, with a regular decrease in thickness and mean grain size with distance.	Emplacement from progressive aggradation from a decelerating, turbulent, stratified current, fed for a short time by a fountaining column. The uppermost accretionary lapilli-bearing, massive, fine ash bed is related to the co-ignimbrite ash cloud.	EU4pf: radial dispersion. Maximum runout up to 21 km in the south. EU7: dispersed mainly to the south. Maximum runout up to 15 km.	EU4pf: −3; 3 EU7: 2	EU4pf: 50%, EU7: 80% Abundant fragments from deep-seated rocks (marble, limestone, skarn, cumulites) as well as lavas from the shallower portions of the conduit.
			Type 3		
EU3pf	Stratified, undulatory bedded to dune bedded deposits locally grading into massive facies. EU3pf deposits drape the topography with an average thickness of up to 1–2 m. They locally show a strong topographic control, thinning on the ridges (down to 5 cm) and thickening in the valleys (up to 5 m). They are formed by pumice lapilli and coarse and fine lithic fragments set in a polymodal matrix of fine and coarse ash. Blocks and bombs up to 20 cm in diameter are present in lens or dispersed in the deposits.	Aggradational sedimentation from a sustained PDC characterized by a depositional boundary layer in which rapid transition from turbulent to non-turbulent deposition locally occurred.	Radial dispersion. Maximum runout up to 10 km away from the eruptive center.	−3; 2	10–40% Fresh lava fragments and minor deep-seated rocks.

Table 1. (continued)

Eruption Unit	Description of the Deposits	Mechanism of Transport and Deposition	Dispersal and Maximum Runout	Mean Grain Size Mdϕ	Lithic Content and Lithology
			Type 4		
EU3pfL	Massive, very thick, up to 10 m, poorly sorted deposits, strongly controlled by topography. They are moderately fine-grained with pumice lapilli and lithic fragments in a polymodal matrix of coarse and fine ash. EU8L has blocks and bombs up to 20 cm in diameter as discontinuous swarms in the middle or toward the top of the bed. EU6 deposits are rich in block-sized lithic ejecta (up to 60% by volume).	Emplaced "en masse" from topographically controlled, non-turbulent, low velocity flows.	EU3pfL: valley filling on the northern and western sectors. Maximum runout up to 5 km. EU6: valley filling on the southeastern slopes of the volcano. Maximum runout up to 6 km. EU8L: valley filling on the northern and western sectors. Maximum runout up to 7 km.	EU3pfL: 0; 1 EU6: −4; −2 EU8L: −1; 1	EU3pfL: 70% EU8L: 40 to 70% Fresh lava fragments from the first 2000 m of subsurface lithology EU6: 60–70% Blocks and boulders from the whole sequence under the volcano
EU6					
EU8L					

[a]Mean-grain size and lithic content data from *Cioni et al.* [1992a, 1999] and *Gurioli et al.* [1999].

were collected primarily in the southern sector. In the northern sector, several samples were taken from deposits of the EU3pfL, the EU4 and the EU8L units (Figure 1a).

[11] At least five lithic fragments were collected from each unit at each site, to give a total of more than 200 clasts. Their lithology includes leucite-bearing lava and scoria, tuff, and rare cumulitic and skarn fragments. More than 30 fragments of Roman tiles were also collected. The fragments were first oriented with both a magnetic and, whenever possible, a solar compass, then removed from the outcrop and successively cored into standard cylindrical specimens (diameter, ϕ = 25.4 mm, height, h = 22.5 mm). Nonoriented samples were collected in some deposits where individual fragments were no larger than 10–15 mm. Apart from the tiles, whose dimensions are standard, the size of lithic fragments collected ranged from 2 to 10 cm in diameter.

3.2. Magnetic Measurements

[12] A JR-5 spinner magnetometer was used to measure both standard and nonoriented specimens. All specimens were thermally demagnetized in 10 to 14 steps using a TSD-2 Schonstedt furnace. After each step, magnetic susceptibility was measured to detect possible mineralogical changes due to heating. Plastic boxes of the type used to sample soft sediments were used to aid measurement of the small bits. Each bit was embedded with white Plasticine in a box to obtain a mold. The bit could then be removed, heated, repositioned and measured in the same position as in the first step. The magnetic noise introduced by white Plasticine is similar to that of the box and is reduced to less than 10^{-4} A m^{-1} by alternating field demagnetization prior to being placed in the box. Because the bits are from strongly magnetized volcanic rocks, the noise level is less than a few percent, even at the end of the thermal demagnetization procedure. Grey Plasticine is strongly magnetic ($\sim 10^{-2}$ A m^{-1}) and is to be avoided. Three types of diagrams were used to analyze the TRM behavior throughout demagnetization (Figure 2):

[13] 1. The normalized intensity decay curve, i.e., the ratio between the remanence intensity measured after each heating step and the initial intensity, describes the path of thermal demagnetization followed by the sample. When used in association with the other diagrams it provides information on the relative intensities associated with the T_b spectra.

[14] 2. The *Zijderveld* [1967] diagram, which is the orthogonal projection of the remanence vector onto the horizontal and either the N-S or the E-W vertical plane, depicts the number of remanence components and shows the temperature values at which they are completely erased.

[15] 3. The Schmidt equal-area projection shows the path of the remanence vector, which is either a point or a great circle depending on whether the remanence consists of one or two components.

4. Results of the TRM Determinations

4.1. General Features of TRM

[16] The TRM of an assemblage of ferromagnetic grains is acquired below the Curie temperature and decays with time because of thermal activation [*Butler*, 1992]. Relaxa-

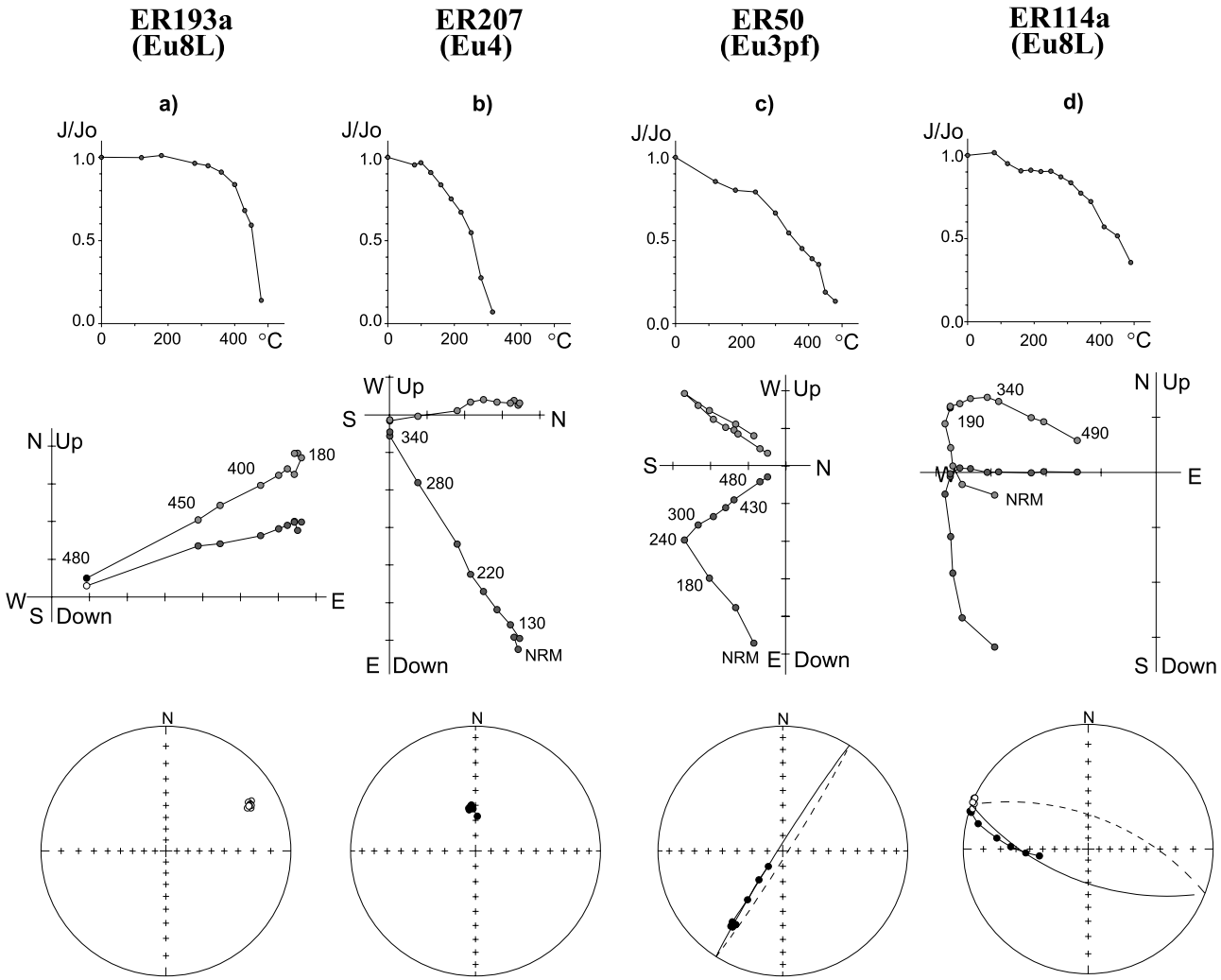

Figure 2. Thermal demagnetization of lithic fragments from the deposits of the Vesuvius A.D. 79 eruption (see text for further explanation). (top) Normalized intensity decay curve, (middle) Zijderveld diagrams (dark dots, declination; light dots, apparent inclination; values, T value (°C)), (bottom) equal-area projection (solid/open dots, lower/upper hemisphere).

tion time increases as temperature decreases, and the blocking temperature, T_b, is defined as the value corresponding to a relaxation time long enough to regard the TRM as stable at geological timescales. The relaxation time also depends on the size and shape of the ferromagnetic grains. The variations of the two parameters yield a distribution of T_b, which is called the T_b spectrum. In the laboratory, because TRM is a reversible process, this spectrum is derived from stepwise thermal demagnetization. Its shape and endpoints record the time during cooling of the rock at which the TRM was acquired.

[17] The lithic and tile fragments could be grouped into four main types of spectra according to the characteristics of their TRM components. Components with $T_b < 150$°C were not included, because their magnetization is indistinguishable from viscous remanence [*Pullaiah et al.*, 1975; *Bardot and McClelland*, 2000].

[18] 1. Type A spectra are shown in Figure 2a. Here the T_b spectrum is narrow and mostly confined to high temperatures. The Zijderveld diagram shows a single-component remanence whose direction does not change throughout demagnetization and differs from the A.D. 79 ambient field direction for the Vesuvius region [*Tanguy et al.*, 1999; *Zanella et al.*, 2000, and references therein]. These fragments still carry their primary TRM, which was not affected by the heat conveyed from the flow. Their directions are randomly oriented because of the chaotic movements of the clasts in the current before they came to rest. Information provided by this type of fragment is limited to a maximum threshold value ($T_{dep} < T_{bmin}$, where T_{bmin} is the lowest T_b value from the spectrum).

[19] 2. Type B spectra are shown in Figure 2b. The T_b spectrum extends from room temperature to ~300°C, which is high enough to remove the whole remanence. This spectra type consists of a single component, whose direction is close to that of the A.D. 79 field. Primary TRM of these fragments was completely erased by syneruptive reheating, and they carry the secondary TRM they acquired as they came to rest and cooled within the pyroclastic deposit. This type of fragment provides a minimum threshold value for the deposition temperature ($T_{bmax} < T_{dep}$, where T_{bmax} is the highest T_b value from the spectrum).

[20] 3. Type C spectra are shown in Figure 2c. Here the Zijderveld diagram consists of two straight-line segments, which correspond to two magnetization components with distinct T_b spectra. The breakpoint in the diagram gives the maximum T_b value ($T_{b\max}$) for the low-T component. The direction of the high-T component is random, whereas that of the low-T component is close to the A.D. 79 field. The two components correspond respectively to the primary TRM and the reheating magnetic overprint. The temperature of the deposit is $T_{dep} \approx T_{b\max}$ and the accuracy of this estimate is determined by the accuracy of defining the breakpoint. This accuracy can be improved either by decreasing the size of demagnetization steps or, when more than one specimen is cut from the same fragment, shifting the steps of one specimen with respect to the other. The breakpoint for the specimen in Figure 2c, for example, lies somewhere between the points 240 and 300°C. That for a twin specimen from the same tile, however, lies between 220 and 260°C. Overlap of the two intervals gives the $T_{b\max}$ boundaries (240°C < $T_{b\max}$ < 260°C) and allows us to estimate T_{dep} with an accuracy of ±10°C.

[21] 4. Type D spectra are shown in Figure 2d. The Zijderveld diagrams of these spectra are similar to that of type C, but the two straight-line segments are connected by a curved path. The two segments still correspond to the high- and low-T components, but their T_b spectra cannot be easily separated. Besides acquisition of the primary TRM and reheating overprint, something else has occurred that makes it hard to trace back to $T_{b\max}$. Various possibilities can be envisaged. For example, mineralogical changes due to syneruptive reheating may result in a chemical magnetization (CRM) overprint [*McClelland-Brown*, 1982] or the fragment may have moved when still hot shortly after deposition (e.g., due to compaction). Resolving this magnetization component often proves impossible because of limited sample material. Lithic fragments within a pyroclastic deposit usually include different lithologies and a fragment is often the only one of its type. A conservative approach is to assume that the range of $T_{b\max}$ has boundaries defined by the highest temperature point that lies on the low-T component segment and the lowest on the high-T segment (190 and 340°C, respectively, in Figure 2d).

[22] Investigation of 201 specimens resulted in 156 $T_{b\max}$ determinations, ~70% from type C fragments and 30% from type D. Most of the remaining 42 specimens had type A spectra.

[23] The reheating temperature of lithic clasts is easier to determine than the deposition temperature of the embedding volcanic unit. The first is the $T_{b\max}$ measured according to routine procedures in the laboratory, whereas T_{dep} is derived from model interpretations of a number of $T_{b\max}$ values. The simplest model assumes hot PDC and cold clasts which exchange heat until thermal equilibrium is reached. All clasts would be heated to approximately the same temperature and T_{dep} could be derived as the mean of the $T_{b\max}$ values. This model is not consistent with experimental data because populations of clasts from individual sites often show a wide range of $T_{b\max}$ values, up to tens of degrees Celsius [*McClelland and Druitt*, 1989; *McClelland and Thomas*, 1993; *Bardot*, 2000; this paper]. The reason is that a PDC is neither a homogenous nor a closed system and thus it continuously exchanges heat with the surroundings. A volcanological discussion of these aspects of the thermal history is given later (section 5); here it is sufficient to remark that a bomb-sized juvenile clast may be substantially hotter than the transporting PDC, whereas a lithic fragment embedded close to the upper surface of the deposit reaches a final temperature lower than that of the PDC. These problems are obviously diminished if one investigates the central portion of a very thick deposit emplaced en masse by a single flow, and enhanced in the case of deposits whose thickness ranges from some decimeters to a few meters, such those of the A.D. 79 eruption. Summing up, the different thermal histories of individual clasts and the variations in the thermal gradient within thin deposits make high-precision determination of $T_{b\max}$ of little use. Moreover, accurate estimates of $T_{b\max}$ are only attainable in the most favorable cases among type C fragments. Evaluation of T_{dep} was therefore carried out following the empirical procedure shown in Figure 3. For each level at each site, the $T_{b\max}$ interval determined for each fragment was plotted and the overlap range of the intervals was assumed to represent T_{dep}. The procedure does not give a mean value and associated error, but it defines the interval that reasonably includes the actual deposition temperature. For most volcanic units of the A.D. 79 eruption, the interval is 20–40°C wide (Figure 3 and Table 2) and T_{dep} is thus estimated with an uncertainty of ±10–20°C. This is small enough to distinguish significant thermal differences in the depositional process of the PDC.

[24] A different approach to the determination of $T_{b\max}$ takes the lowest temperature found at a site as a record of T_{dep}, and considers the higher values to be related to preheated fragments [*McClelland and Thomas*, 1993]. This approach, however, assumes a PDC to be a thermally closed system and is not applicable to very thin deposits. In the present paper only five fragments are characterized by $T_{b\max}$ values lower than the overlap interval, with no more than one sample per site (Figure 3); these were considered to be outliers. The data from Ercolano-EU3pf suggest two tentative explanations for these outliers. At this site, one out of seven tiles yields a temperature some tens of degrees Celsius lower than the others. Either the temperature was homogenous throughout the deposit and six tiles were preheated immediately before being embedded in the flow or one tile was embedded in a colder, peripheral portion of the deposit and reached a lower final temperature. The first hypothesis is hardly tenable, whereas the second is consistent with the small thickness (~150 cm) of the deposit.

4.2. Overprint Magnetization

[25] If the overprint magnetization resulted from syneruptive reheating of the fragments, its direction should be close to that of the ambient magnetic field at the time of cooling. The mean overprint direction for each site was calculated from all the fragments irrespective of the level they are embedded within each deposit, as the deposition and cooling times were negligible with respect to the timescale for secular variation. Table 3 and Figure 4 show a very limited dispersion around a mean direction (declination, D = 354.4°, inclination, I = 57.2°; Fisher's precision parameter k = 433, semiangle of confidence α_{95} = 2.7°) close to that derived from fine-grained pyroclastic products of the A.D. 79 eruption (D = 355°, I = 59°) and archae-

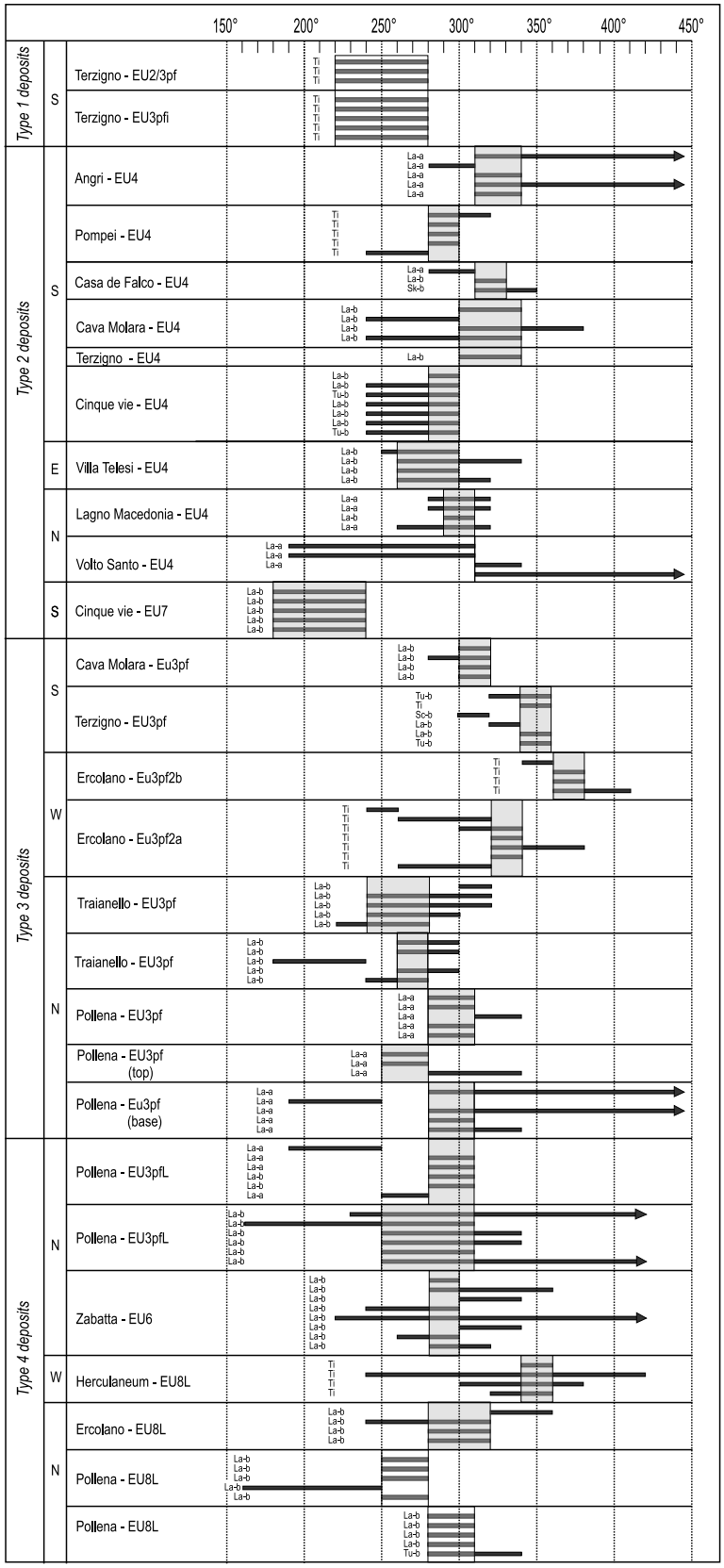

Figure 3. Evaluation of the A.D. 79 PDC deposits temperature (T_{dep}), by overlap of individual clast reheating temperature ranges (see text for further explanation). The arrows indicate values higher than 450°C. The lithology and dimensions of the lithic clasts are shown: Ti, tile; La, lava; Sk, skarn; Tu, tuff; Sc, scoria; a, lithic fragment with diameter less than 2 cm; b, lithic fragment with diameter larger than 2 cm and less than 10 cm. Tile fragment dimensions are standard.

Table 2. Temperature of PDC Deposits of the A.D. 79 Eruption[a]

Site	Section Sector	D, km	EU	SU	n	T_{dep}, °C	Unit Thickness, cm	Mdϕ	$L > 1$ mm, %	$J < 1$ mm, %
					Type 1					
Terzigno	7 S	6.3	EU2/3pf		3	220–280	10	0	6.15	-
Terzigno	7 S	6.3	EU3pfi		5	220–280	25	−2	-	-
					Type 2					
Angri	42 S	15	EU4		5	310–340	9	3	-	-
Pompei	14 S	9.5	EU4		8	280–300	30	2	2.47	21.81
Casa de Falco	60 S	6.2	EU4		5	310–330	130	2	-	-
Cava Molara	6 S	3.9	EU4		6	300–340	200	0	-	-
Terzigno	7 S	6.3	EU4		1	300–340	67	1	3.97	59.60
Cinque vie	40 S	6.3	EU4		7	280–300	200	-	-	-
Villa Telesi	4 E	4.7	EU4		5	260–300	60	2	-	-
Lagno Macedonia	47 N	5.25	EU4		4	290–310	34	-	-	-
Volto Santo	26 N	4	EU4		4	310	100	0	-	-
Cinque vie	40 S	6.3	EU7		5	180–240	69	2	-	-
					Type 3					
Cava Molara	6 S	3.9	EU3 pf		7	300–320	150	1	-	-
Terzigno	7 S	6.3	EU3pf		12	340–360	30	0.5	-	-
Ercolano	61 W	7	EU3pf	2b	8	360–380	250	−0.5	0.00	39.58
Ercolano	61 W	7	EU3 pf	2a	12	320–340	150	−1	3.78	34.20
Traianello	47c N	5	EU3pf	3	8	240–280	300	-	-	-
Traianello	47c N	5	EU3pf	1	6	260–280	200	-	-	-
Pollena	54 N	4.6	EU3pf	3	5	280–310	40	2	-	-
Pollena	54 N	4.6	EU3pf	2top	3	250–280	40	1	-	-
Pollena	54 N	4.6	EU3pf	2base	5	280–310	40	−1	9.65	-
					Type 4					
Pollena	54 N	4.6	EU3pfL	2	6	280–310	100	0	17.40	-
Pollena	54 N	4.6	EU3pfL	4	8	250–310	300	0	10.44	-
Zabatta	3 N	4.8	EU6		14	280–300	2000	−2	-	-
Ercolano	61 W	7	EU8L	1	4	340–360	60	0	11.61	-
Traianello	47c N	5	EU8L	1	9	280–320	600	-	-	-
Pollena	54 N	4.6	EU8L	2	5	250–280	100	−1	-	-
Pollena	54 N	4.6	EU8L	1	10	280–310	300	−1	-	-

[a]Site and section data are as in Figure 1; D, distance from the vent; EU, eruptive unit, and SU, subunit, according to the terminology of *Cioni et al.* [1992a]; n, number of temperature determinations; T_{dep}, deposit temperature; Mdf, *Inman* [1952] mean diameter; L, lithic fragments larger than 1 mm; and J, juvenile fragments smaller than 1 mm.

omagnetic materials from Pompei and Ercolano ($D = 358°$, $I = 59°$) [*Tanguy et al.*, 1999; *Zanella et al.*, 2000, and references therein]. The data in Table 3 only refer to 8 sites and 87 fragments taken from a total of 159 fragments from 11 sites. The reason for this discrepancy is that in some flow units and/or at some sites lithic fragments were too small to be accurately oriented. Hence their directions could not be safely transformed to the geographical reference system and were discarded from calculation of the mean site directions. Note that this lack of accuracy does not prevent evaluation of $T_{b\max}$, which is given by the breakpoint between the overprint and primary magnetization directions. Because $T_{b\max}$ does not depend on the reference system it is not affected by orientation errors.

[26] As far as we know, small bits have not previously been used to derive deposition temperature of PDCs. We thus completed our analysis as a trial approach for studying those sites lacking of larger fragments. However, this approach means that a significant comparison between the results obtained from lithics of different size cannot be made. The overall results (Figure 3), however, give no evidence to doubt the quality of the results and suggest that collection of both small and large fragments at the same site could provide a deeper insight into the thermal history of a PDC.

[27] The most precise temperature determinations were obtained from the Roman tiles. This is probably due to the fact that they acquired both primary and overprint magnetizations through similar processes (firing in a furnace and reheating within the pyroclastic deposit respectively). To assess their reliability as archaeomagnetic thermometers, the acquisition process was repeated in the laboratory on some tiles. The experiment (Figure 5) was carried out as follows:

[28] 1. The NRM was first measured; its intensity was $J = 3.57$ A m^{-1}.

[29] 2. The A.D. 79 overprint was erased by a single step demagnetization at 350°C. The intensity of the remaining high-T component was $J = 1.78$ A m^{-1}, and its direction in the specimen reference system was $D = 14°$, $I = 36°$.

[30] 3. The specimen was placed inside an unshielded oven whose ambient field direction ($D = 208°$, $I = 78°$ in the specimen reference system) had previously been measured with a triaxial fluxgate magnetometer. After reheating to 350°C, it was allowed to cool and remagnetize. The remanence intensity after cooling was $J = 3.39$ A m^{-1}.

[31] 4. Last, the specimen was demagnetized in 12 steps. The laboratory magnetic overprint ($D = 205°$, $I = 76°$) was close to the ambient field and fully removed after heating to 350°C. The remanence measured after this step ($J = 1.77$ A m^{-1}; $D = 8°$, $I = 37°$) was indeed like the high-T component measured at point 2 ($J = 1.78$ A m^{-1}; $D = 14°$, $I = 36°$).

Table 3. Site Mean Directions of the Overprint Thermal Magnetization of the Vesuvius A.D. 79 Eruption Deposits[a]

Site	n	D, I	k	α_{95}
Casa de Falco	8	0.4, 58.0	84	6.1°
Cava Molara	11	345.1, 52.9	19	10.9°
Ercolano	25	351.0, 59.8	55	3.9°
Pollena	14	358.3, 55.8	34	6.9°
Sezione 40	8	352.6, 58.3	55	7.5°
Terzigno	9	2.7, 59.8	44	7.8°
Traianello	6	353.0, 56.8	144	5.6°
Zona Zabatta	6	353.3, 55.4	67	8.2°
All sites	8	354.4, 57.2	433	2.7°

[a]Symbols: n, number of lithics; D, I, declination, inclination; k, Fisher's precision; α_{95}, semiangle of confidence.

[32] The results from this experiment, together with a few others in the literature [*Evans and Mareschal*, 1986; *Marton et al.*, 1993], show the utility of tiles in unraveling the thermal history of archaeological sites.

4.3. Role of the Kinetics of TRM Acquisition

[33] A process that is often overlooked when discussing the results of T_{dep} determination from TRM analyses concerns the kinetics of TRM acquisition. The timescale of cooling of fragments embedded in a PDC deposit depends on the cooling history of the deposit itself. According to *Riehle et al.* [1995], the timescale of cooling of a thick deposit (days, months) is completely different from that of a thinner deposit (hours). On the other hand, the timescale of experimental thermal demagnetization is generally predetermined, and of the order of minutes or hours. Because T_b can be considered as an energy threshold, and the probability that this threshold can be crossed is a function of temperature, the timing of magnetization acquisition during cooling overlaps with that needed for thermal demagnetization. As a result, the complete obliteration of the TRM acquired during very slow cooling of the fragment will be attained at higher temperatures during the more rapid, laboratory heating. In other words, the T_b value obtained in the laboratory will be a more accurate proxy of the deposit temperature for those fragments that cooled most quickly than for those that cooled slowly.

4.4. Temperatures of the A.D. 79 PDC Deposits

[34] The emplacement temperatures estimated for the A.D. 79 PDC deposits fall in the range of 180–380°C, although most of the samples show temperatures spanning 240–340°C (Figure 3). This spread is present both in the deposits of the same eruptive unit sampled at different sites, and among deposits derived by PDCs with similar physical characteristics (Table 2 and Figures 3 and 6). Using these results, we may state some general points.

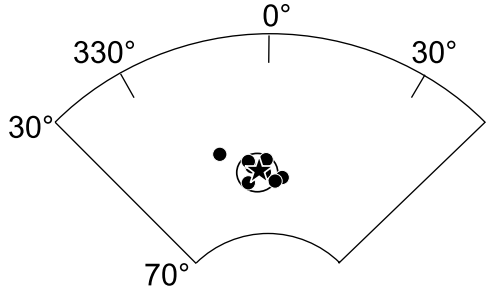

Figure 4. Equal-area projection of the site-mean directions of the overprint magnetization. Star is Vesuvius A.D. 79 mean direction with circle of confidence.

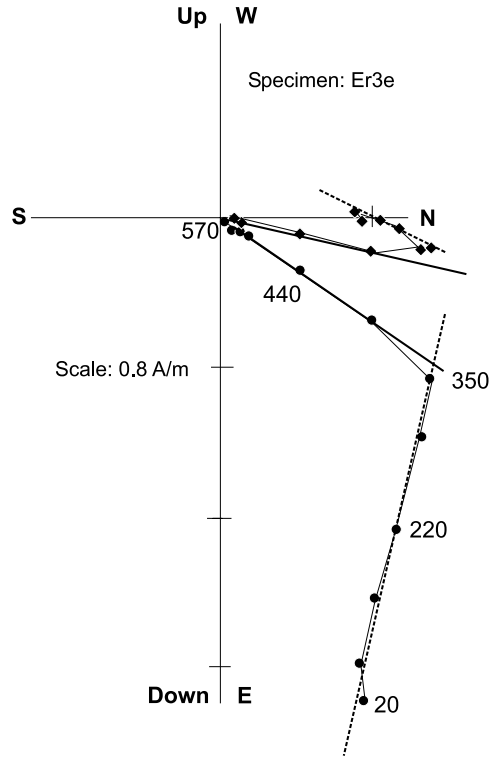

Figure 5. Zijderveld diagram for thermal demagnetization of a tile fragment reheated in the laboratory. Dot, declination; diamond, apparent inclination; dashed line, low-T component; heavy line, high-T primary component. See text for further explanation.

[35] 1. No regular trend of temperature variation is observed throughout the stratigraphic sequence.

[36] 2. The differences in temperature observed between samples collected from different types of PDC are statistically significant, especially those related to type 1, 2, and 3 deposits (Table 2 and Figure 3).

[37] 3. Both type 2 and 3 deposits show temperatures spanning a large interval. This interval is strongly reduced when the deposits are related to the sector of provenance (south versus north and east, Figure 3), with PDC deposits from the southern sector having the highest temperatures.

[38] 4. Type 4 deposits show the largest variability of temperature at the scale of individual sampling sites.

[39] The samples collected inside the Ercolano excavations show the highest temperatures, up to 380°C (Table 2 and Figures 3 and 6). They are higher than the combustion temperature (around 300–320°C) of some papyri remains found at Villa dei Papyri, a newly excavated area very close to the Ercolano ruins [*Basile*, 1994], but lower than the PDC temperature of about 500°C, indicated by *Mastrolorenzo et al.* [2001].

[40] The lowest temperatures (180–240°C) are recorded by fragments taken from the lithic-rich, phreatomagmatic type 2 deposits of EU7 (Table 2). Low temperatures of around 250°C have also been determined for type 1 deposits

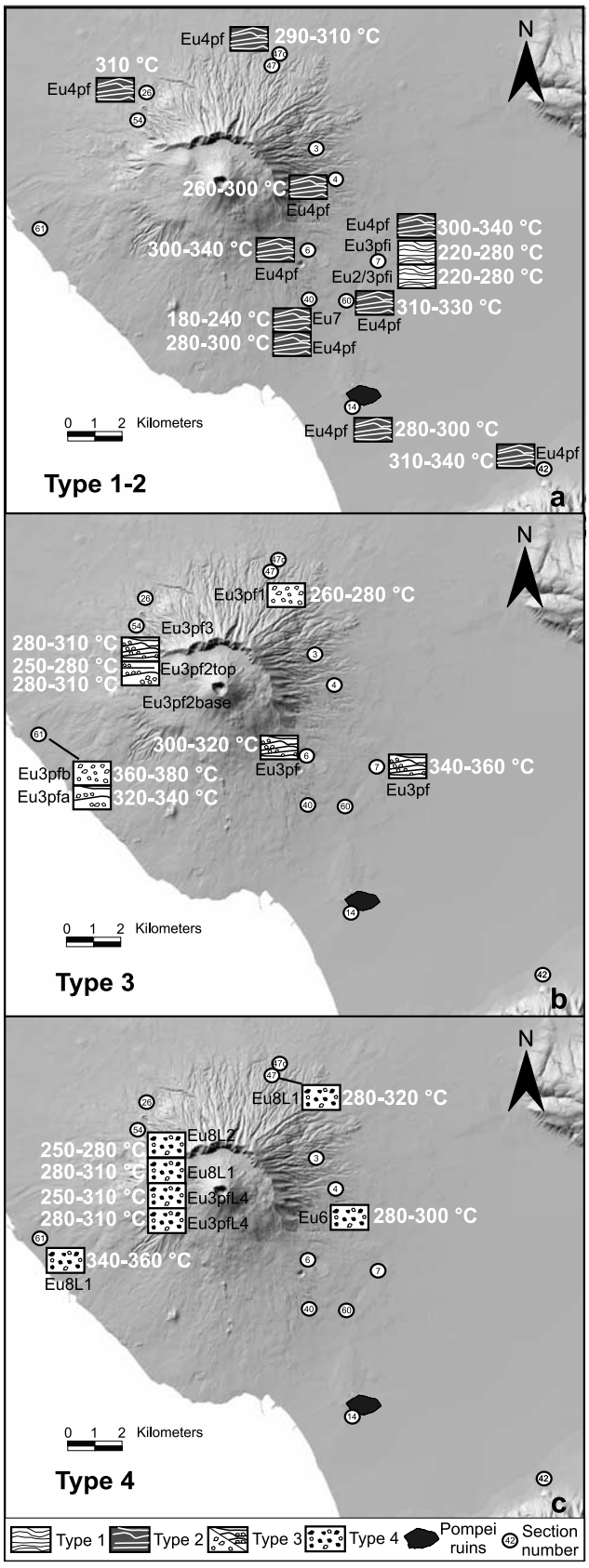

Figure 6. Estimated temperatures of the A.D. 79 deposits as a function of the site locations and the type of the PDC deposits.

of the magmatic phase (EU2/3pf and EU3pfi; Figure 1 and Table 2). In these deposits, because of the scarcity of coarse lithics, temperatures were measured only on tiles picked up from the roofs of Roman buildings by the PDC.

[41] The type 2 deposits of EU4 generally have higher temperatures and a bimodal distribution with peaks around 290 and 320°C, corresponding to the different provenance of the samples (Table 2 and Figure 6). The same range of temperature can be observed in both lithic fragments and roof tiles. For this unit, samples collected at different distances from the vent do not show systematic temperature variations.

[42] The temperature of type 3 deposits, represented only by the EU3pf, varies between 260 and 340°C (Table 2). As for EU4, the main differences can be traced back to the sectors of provenance of the samples (northern versus southern slopes of the volcano).

[43] The type 4 deposits, mainly related to the final phreatomagmatic phases of the eruption, give temperatures clustered between 260 and 300°C, similar to the lowest values measured in the EU3pf.

5. Discussion

5.1. Volcanological Significance of TRM Data

[44] The temperature within a PDC is not homogeneous during its very short flow duration, because the different components (lithics and juvenile fragments, magmatic gases and external fluids, such as water and air) are incorporated in the flow at different times and temperatures. Attainment of thermal equilibrium between the different constituents depends on their relative mass, time of residence, thermodynamic properties and size of the fragments. At any time, the temperature of the flowing PDC should therefore be defined as the average temperature of all its components, weighted according to their abundance. To a first approximation, the ash-grade juvenile fragments often represent the largest mass fraction in the current (>80% by weight) and can be considered thermally and mechanically coupled with the carrying gas [*Sparks*, 1976; *Druitt*, 1998]. We can thus assume that the PDC temperature is approximated by the temperature of the gas-ash mixture. The process of attainment of thermal equilibrium between the different constituents of a PDC can be understood in terms of the timing and energy budget of heat exchange between a large source (the ash-gas mixture) and individual fragments.

[45] For paleotemperature studies, TRM analyses are generally performed on coarse lithic or pumice clasts (see *McClelland and Thomas* [1993] for a discussion). Lithic clasts coarser than several cm's in diameter should be avoided because they do not attain a homogeneous internal temperature distribution [*Marti et al.*, 1991; *Bardot*, 2000].

[46] The thermal history of coarse fragments transported and deposited by a PDC depends on the factors controlling the temperature of the flowing current and the cooling history of its deposit. The PDC cools progressively during flow, essentially because of air ingestion and heat transfer to the cooler lithic fragments. After deposition, the cooling history depends on the thickness of the deposit [*Riehle et al.*, 1995; *Miller*, 1990]. Different constituents follow a thermal evolution which depends on their physical properties, initial temperature, size and position inside the deposit. All these factors are discussed in the context of their

importance in determining the temperatures of the A.D. 79 Vesuvius deposits.

5.1.1. Initial Magma Temperature

[47] The temperature of the magma at eruption defines the initial temperature of the gas-ash mixture in the PDC where the magmatic gases as well as the coarse- and fine-grained juvenile fragments in the erupting mixture can be considered in thermal equilibrium at eruption [*Dobran and Papale*, 1993]. The coarse fragments rapidly decouple from the mixture, because of their different thermal inertia with respect to the other juvenile components. The temperature of the coarse juvenile material will generally decrease at a slower rate than the mixture of gas and ash.

[48] Direct estimations of magma temperature for the A.D. 79 products were made by *Barberi et al.* [1981] and *Cioni et al.* [1995]. They determined the magma temperature to be around 850°C. Composition-dependent variations in the temperature during the eruption proved to be minor. For this reason, the initial temperature of all A.D. 79 PDCs can be considered constant.

5.1.2. Lithic Content

[49] *Marti et al.* [1991] suggested that the amount of lithic fragments carried by a PDC is crucial in determining its final temperature. In particular, only those lithic fragments with a characteristic Fourier number τ ($\tau = kt/a^2$, where k is the lithic thermal diffusivity, t is the time of heat exchange and a is the lithic radius) greater than 1 (corresponding to an energy transfer of 97%) can reach thermal equilibration within the flow. If they are cold at the moment of their entrainment, they can help to decrease the final temperature of the flow. Because of the comparable heat capacity of lithic and juvenile material, only the presence of a large amount of lithic fragments can be effective in decreasing the PDC temperature. For typical values of k (of the order of 0.01 $cm^2\ s^{-1}$ [*Jaeger*, 1968]) and $t > 300$ s (an acceptable approximation for the total duration of flow in the conduit, the atmospheric path and the emplacement time), all the lithic clasts with a radius smaller than 1 cm will reach thermal equilibration within the flow before deposition. Clasts of these dimensions generally represent the majority of the lithic fragments carried by the erupting mixture (see, for example, the data on components of the A.D. 79 deposits of *Barberi et al.* [1989] and *Gurioli* [2000]).

[50] An overlooked feature of fine-grained lithic fragments is the possibility that they were partially heated before entering the magmatic mixture. This effect can be particularly important when lithic fragments are eroded from the conduit walls rather than from the vent area, because of the heating effect of the erupting mixture on the conduit walls during its ascent to the surface. As a result, incorporation of "preheated" lithic fragments would cause only a minor thermal perturbation of the carrying mixture.

[51] Assuming a progressive enlargement of the conduit, *Varekamp* [1993] estimated an average erosion rate of around 5 m h^{-1} for the Plinian phase of the A.D. 79 eruption. The timescale of the contact between the erupting magmatic mixture and the conduit walls, from which lithic fragments a few millimeters across were continuously eroded, is only a few seconds. Considering heat exchange for a liquid at constant temperature flowing through a cylindrical conduit within a homogeneous infinite medium, and neglecting any possible viscous heating effect, the temperature gradient from the conduit walls outward can be calculated at different times [*Carlsaw and Jaeger*, 1959, pp. 335–336]. Figure 7 shows that for a continuously flowing mixture at 850°C in a 50 m radius cylindrical conduit, with a thermal diffusivity of the host rocks of 0.01 $cm^2\ s^{-1}$, an annular collar of a few millimeters in width reaches temperatures in excess of 400–500°C after only 5 s. This suggests that at least some of the fine-grained lithic fragments eroded from the conduit walls could have been thermally coupled with the erupting mixture at the moment of their incorporation, thus increasing the average temperature of the lithic fraction incorporated in the mixture and decreasing the induced thermal disturbance.

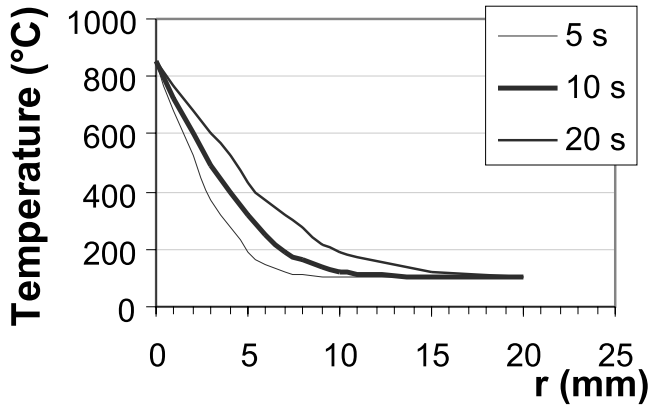

Figure 7. Temperature variation with time of an annular collar around a conduit with a radius of 50 m and occupied by a flowing mixture at 850°C. After only a few seconds, a thin collar a few millimeters across reaches a temperature higher than 400–500°C, suggesting that small fragments eroded from the conduit walls may be close to the thermal coupling with the erupting mixture at the moment of their incorporation.

[52] On average, components of the A.D. 79 PDC deposits [*Barberi et al.*, 1989; *Vecci*, 1992; *Gurioli*, 2000] yields a total lithic content of about 20–30% by weight, with most fragments smaller than 1 cm. Furthermore, the lithologic features of the different fragments suggest that most were derived from deep portions of the plumbing system (magma chamber walls and conduit [*Barberi et al.*, 1989]). This suggests that, for most A.D. 79 PDCs, a large proportion of the total lithic population was probably hot.

[53] On the other hand, the results of the calculations illustrated in Figure 7 indicate that the initial temperature of the lithic fragments larger than several centimeters (like those used for TRM analyses) can be approximated by the temperature defined by the local geothermal gradient at their depth of provenance, and excluding the possibility of an important preeruption demagnetization.

5.1.3. Air Ingestion During Flow

[54] Air ingestion and heating are fundamental processes governing the generation and transport of PDCs [*Sparks*, 1976; *Druitt*, 1998]. During the ascent of a gas-pyroclast mixture in an erupting fountain, substantial air ingestion occurs at the top of the gas thrust region [*Sparks et al.*, 1997]. Even though air entrainment in the collapsing fountain is not fully understood [*Bursik and Woods*,

1996], an upper limit to the amount of air ingested can be made using the results of the model of *Dobran et al.* [1993]. This suggests that a lower temperature limit of the collapsing mixture is around 800°C.

[55] Air ingestion during the flow of the current is described by the Richardson number of the cloud, *Ri*. This is the ratio between the buoyancy and kinetic energy of the PDC ($Ri = [\beta - \alpha]\, gh_{PDC}\beta/u^2$, where α and β are the air and current densities respectively, g is the acceleration due to gravity, h_{PDC} is the thickness, and u is the velocity of the current). *Bursik and Woods* [1996] suggested that air ingestion is highly effective in supercritical currents characterized by high velocities and $Ri < 1$. In such currents, the progressive deposition of material from the cloud and the continuous turbulent engulfment of air decrease the cloud density (β), substantially decreasing *Ri* and maintaining the current in a supercritical regime. *Bursik and Woods* [1996] conclude that supercritical ash flows show a temperature decrease with run-out distance larger than that of subcritical currents, in which turbulence is suppressed and air ingestion strongly reduced.

[56] Air ingestion has a strong effect on the final thermal state of the cloud. The very high thermal diffusivity (k) of air with respect to magma ($k_{air}^{298\ K} = 2.37 \times 10^{-1}$ cm^2 s^{-1}; $k_{magma} = 10^{-2}$ cm^2 s^{-1}) and the intimate mixing between the air and the gas-ash mixture results in instantaneous thermal equilibration. Additionally, the mass of ingested air can be of the same order as that of the transported solids (several tens of percent [*Bursik and Woods*, 1996]) and it thus plays an important role in the thermal history of the cloud. All these relationships must be kept in mind when discussing the thermal history of the dynamically complex A.D. 79 PDCs.

5.1.4. Involvement of External Water

[57] The thermal effects of adding low-temperature external water to an erupting mixture have been discussed in detail by *Koyaguchi and Woods* [1996]. The larger specific heat capacities (Cp) of water and vapor with respect to magma ($Cp_{water}^{298\ K} = 4.18$ J g^{-1} K^{-1}; $Cp_{vapor}^{398\ K} = 2.04$ J g^{-1} K^{-1}; $Cp_{magma}^{1200\ K} = 1.3$ J g^{-1} K^{-1}) and the very high value of the latent heat needed to vaporize water ($\Delta H_{vap} = 2250$ J g^{-1}) make water-magma interaction the most efficient way to reduce the temperature of the erupting cloud. This could be one of the most important factors in the thermal history of some of the A.D. 79 deposits, because the involvement of phreatic water during the final phases of the eruption is generally accepted, with only some controversies remaining regarding the onset of the process [*Sheridan et al.*, 1981; *Sigurdsson et al.*, 1985; *Barberi et al.*, 1989]. The complete vaporization of only a few weight percent of liquid water can decrease the temperature of the PDC by hundreds of degrees. External water may also interact with the still hot deposit in the form of rain or moisture released by the heated substratum. In such cases, water will be the main factor controlling the cooling rate of the deposit. Unfortunately, the importance of these factors on the final cooling path of the fragments cannot be assessed.

5.2. Timing of Thermal Equilibration Between Clasts and the Gas-Ash Mixture: Importance of the Cooling History of the Deposit

[58] Whereas the temperature of the bulk of a PDC (gas and fine-grained fragments) decreases during flow because of progressive admixing of air, the thermal evolution following deposition is more important for the coarsest fragments. Assuming a spherical lithic clast of radius r placed in an infinite medium at time $t = 0$, where a clast of temperature T_0 is surrounded by a medium at temperature T_e, then the heat transfer can be calculated following *Carlsaw and Jaeger* [1959]. Using this solution [*Bardot*, 2000, equation (1)], it is possible to estimate the time for thermal equilibration between the gas-ash mixture and the coarser fragments (Figure 8). Making rough assumptions about the mean velocity (around 50–100 m s^{-1} [*Druitt*, 1998]) and the maximum observed run-out (10–15 km) of the current, the lifetime of a flowing PDC can be estimated at 100–200 s. This can be considered as the residence time for fragments transported in the high-temperature gas-ash mixture. If the mixture temperature is assumed constant during heating of the fragments, the time required for thermally equilibrating lithic fragments between 2–5 and 10 cm in radius is generally larger than the timescale of residence in the flow. In particular, for mixture temperatures between 400 and 600°C, lithic clasts with a radius larger than 2 cm equilibrate after a very prolonged contact with the gas-ash mixture (Figure 8). As the fragments used for the TRM measurements are generally larger than several centimeters across, the measured temperatures represent the temperature reached by the clast in the deposit rather than that of the PDC during emplacement. An extreme situation is represented by measurements performed on the roman tiles, which were entrained cold in the flowing cloud and rapidly dropped and heated in the deposit.

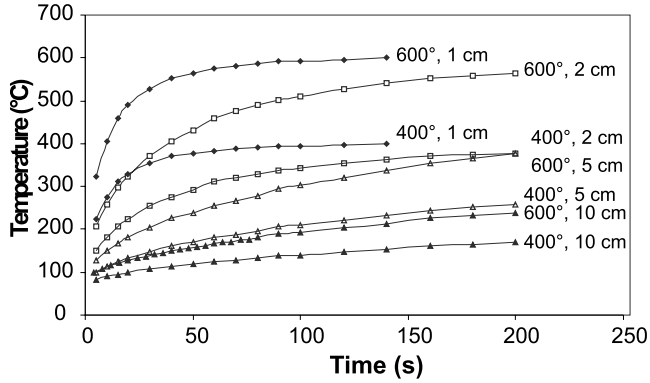

Figure 8. Temperature variation with time for spherical lithic fragments with radii between 1 and 10 cm in a high-temperature mixture (assumed constant during heating of the fragments). For mixture temperatures between 400 and 600°C, the time taken for the lithics larger than 2 cm in diameter to reach equilibrium following contact with the gas-ash mixture is much longer than the PDC run-out time. The thermodynamic properties of the fragments are discussed in the text; the heat transfer equation used in the calculation is from *Carlsaw and Jaeger* [1959] and *Bardot* [2000].

[59] Figure 9 shows the thermal history of juvenile and lithic coarse fragments during transport and following deposition from a hypothetical PDC. The temperature of the PDC is assumed to vary rapidly during flow (from 600° to 400°C) because of efficient turbulent admixing of air in the cloud, while the cooling history of the whole deposit is assumed to be similar to that observed for small-scale PDC

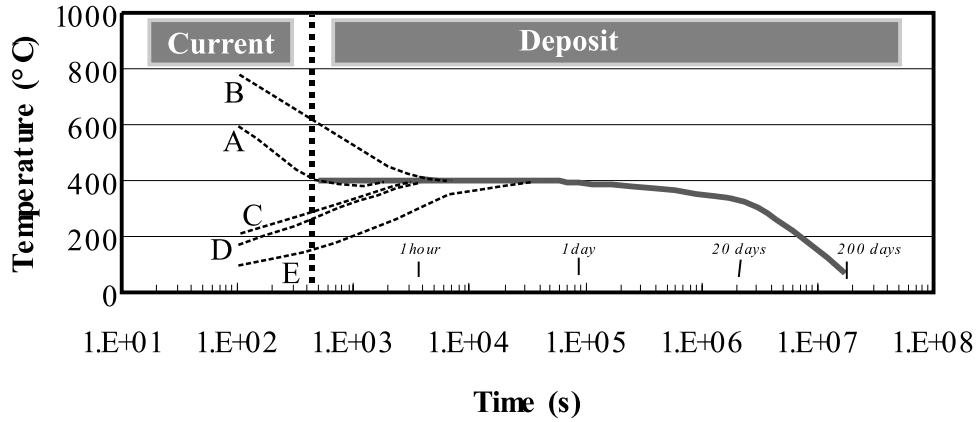

Figure 9. Thermal history of juvenile and lithic coarse fragments during transport and after deposition from a small PDC, characterized by a temperature decrease from 600° to 400°C due to very efficient air incorporation. The cooling history of the deposit is derived from temperature measurements taken on small-sized PDC deposit by *Kozu* [1934] and *Ryan et al.* [1990] and from the thermal modeling proposed by *Miller* [1990] and *Riehle et al.* [1995]. Both juvenile and lithic coarse fragments reach complete equilibration with the whole deposit several hours after deposition. The thermodynamic properties of the different constituents are presented in the text. The thermal history of each single clast up to equilibration with the flowing PDC or the deposit is derived with the same assumptions as in Figure 8.

deposits [*Kozu*, 1934; *Ryan et al.*, 1990], and to the thermal modeling proposed by *Miller* [1990] and *Riehle et al.* [1995]. The main result of these calculations is that coarse juvenile and lithic fragments completely equilibrate with the rest of the deposit one to several hours after deposition. In particular, while coarse lithic fragments are continuously heated to reach a maximum temperature (corresponding to the temperature of the embedding ash at the time of equilibration; Figure 9), the coarse juvenile fragments act as a heat source for the deposit. This behavior becomes particularly important in the presence of a rapidly cooling deposit, as for example a very thin bed or a deposit cooled by strong air convection or by syneruptive rain. A corollary is that coarse lithic fragments very close to the upper, rapidly cooling surface or embedded in a very thin deposit, can give temperatures lower than the mean PDC temperature at deposition. On the other hand, if a fragment is well inside the bed, or is set inside a very thick sequence of syneruptive deposits, it reaches thermal equilibrium with the embedding medium rapidly with respect to the long cooling time of the deposit.

6. Temperature of the A.D. 79 PDCs: Inferences From TRM Data on the Deposits

[60] The TRM data highlight some temperature variations that can be discussed in terms of average and local processes of transport and deposition, as suggested by the sedimentological and compositional features observed in the different types of PDC deposits (Table 1).

6.1. Type 1 (Thin, Fine-Grained, Cross-Stratified PDC Deposits)

[61] These deposits are represented by EU2/3pf and EU3pfi (Table 1 and Figures 1a and 1b). They correspond to the lowest temperatures (from 220 to 280°C, Figures 3 and 6) for any of the products of the magmatic phase of the eruption. When interpreting such low values we should bear in mind the sedimentological features of these lithic-poor, fine-grained, thinly laminated deposits (Table 1). There are two possible explanations for the TRM results.

[62] 1. The low temperatures are related to a low initial temperature of the current, representing detachment and collapse of the marginal, fines-rich portions of the eruptive column. In this case, the cool character of the mixture is directly related to extensive, turbulent ingestion of air in the collapsing column. The rapid thermal equilibration in the flow, resulting in a decrease of the average temperature of all its constituents, was driven by the fine grain size of the hot pyroclasts and by the high thermal diffusivity of the gas. The estimated temperature should be very close to the average temperature within the flow at deposition because of the abundance of only fine-grained fragments transported in the PDC.

[63] 2. The low temperatures measured on the lithic fragments derive from the rapid cooling of these thin deposits, competing with the postdeposition heating of the lithic fragments. This is especially true in the case of the measurements made on the tile fragments, cold at the moment of incorporation in the PDC and rapidly incorporated into the deposit.

6.2. Type 2 (Thick, Fining Upward Massive to Stratified PDC Deposits)

[64] EU4 and EU7 represent two different types of deposits derived from stratified, turbulent PDCs (Table 1). The main differences observed in the two deposits are the very different lithic content (50 versus 80% by weight in EU4 and EU7, respectively; Table 1) and the contrasting textural features of the juvenile fraction (abundant, highly

vesicular in EU4; sparse, dense and crystal rich in EU7 [*Cioni et al.*, 1992b]). *Cioni et al.* [1992a] also showed that EU4 deposits are characterized by component and morphological features of the juvenile material somewhat transitional between those of the magmatic deposits of the Plinian phase and those of the final, phreatomagmatic, accretionary lapilli-bearing deposits. They concluded that EU4 probably marked the onset of phreatomagmatic activity in the eruption, related to the first destabilization of the shallow magma system. In contrast, EU7 deposits have unequivocal evidence for significant magma-water interaction (prevalently dense juvenile material, high lithic content, external morphology of the juvenile fragments characterized by adhering particles, overgrowths of secondary minerals and rare hydration cracks). In the eruption reconstruction of *Barberi et al.* [1989] and *Cioni et al.* [1992a] this was interpreted to be related to a progressive increase of the water to magma ratio during the final phase of the eruption.

[65] Samples from EU4 were collected at 9 different sites, between 4 and 15 km from the vent (Figure 6). All sites yielded temperatures around 300°C, irrespective of their distance from the vent. However, as already discussed, samples from the northern sector have slightly lower temperatures than those from the southern sector.

[66] The fairly uniform temperature measured on EU4 samples at the different sites suggests substantial homogeneity of the transporting system, in agreement with the limited control exerted by topography on the distribution of the EU4 deposits [*Cioni et al.*, 1992b; *Gurioli*, 2000]. Because the PDC can be considered a density stratified current [*Valentine*, 1987] with a basal coarse-grained portion characterized by a high concentration, the thermal homogeneity within the flow is continuously maintained because of the low efficiency of air incorporation, the fine-grained character of the majority of the transported material and the continuous settling of the coarsest, thermally unequilibrated fragments toward the basal portion of the PDC. This agrees with the results of *Dobran et al.* [1993], which show constant temperatures in the basal few meters of the currents [*Dobran et al.*, 1993, Figure 10].

[67] Air ingestion during flow was possibly important at sites where the presence of obstacles induced locally enhanced turbulence and decreasing the temperature of the PDC. This is evident at Pompei (section 14, Figure 6) for samples collected just down flow from some archaeological remains, where the sedimentological features of the EU4 deposits suggest a local, sharp increase in turbulence and a decrease of mean particle concentration of the cloud [*Cioni et al.*, 1996]. Incorporation of 10% by weight of cold air with respect to the mass of the PDC could explain the slightly lower temperature observed at Pompei.

[68] The temperatures measured on the samples from the most distal section (15 km from the vent, section 42 in Figure 6) are close to the average value of the other sections and higher than those at Pompei confirming that, on average, the temperature of the current did not significantly decrease during the flow.

[69] Whereas the PDCs seem to have maintained a nearly constant temperature in a large part of the southern sector, to the north, just down flow from the preexisting walls of the Somma caldera, the TRM data suggest some major perturbations (Figure 6). In this northern sector, samples collected at 5–6 km from the vent (sections 4 and 47, Figure 6) have average temperatures 30–40°C lower than those estimated from samples collected at equivalent distances from the vent in the southern sector (sections 6, 7, 40 and 60, Figures 3 and 6). We relate the general northerly temperature decrease to the impact of the PDCs with the caldera walls, inducing premature settling of material and favoring air incorporation. This is also in agreement with the results of numerical modeling [*Todesco et al.*, 2002].

[70] EU7 deposits (Table 1) show sedimentological features similar to EU4, but a very different components related to the clear phreatomagmatic character of the current. TRM determinations from samples collected at one site (Figure 6) give the lowest temperatures of the whole sequence (210 ± 30°C). We suggest two possible explanations for these low temperatures, respectively related to the very high lithic content of the deposits or to a very efficient (in terms of thermal exchange) magma-water interaction. Given that a large proportion of the lithic fragments were probably already hot because they derive from the deep seated, hot rocks close to the magma chamber (skarns, cumulates, thermometamorphic marbles), we suggest that the low temperature associated with these deposits (about 100°C lower than the average temperature shown by the EU4 deposit at the same site) records the strong thermal effect of phreatic water incorporation in the PDC. Assuming a system similar to the EU4 current, complete vaporization of a very low amount of low-T water (3–4% by weight of the total, for pure water at 60°C), calculated according to the analysis of *Koyaguchi and Woods* [1996], is sufficient to explain the difference in the temperature between the EU4 and EU7 deposits. Even if this is a lower limit to the amount of external water incorporated into the erupting mixture, this result stresses the importance of magma-water interaction in determining the final temperature of PDCs and the high efficiency of this process.

6.3. Type 3 (Thick, Stratified Deposits Laterally and Vertically Grading Into Massive PDC Deposits)

[71] The EU3pf deposits show a wide temperature range, from 240 to 360°C. As samples were collected in a narrow belt all around the vent (at distances between 4 and 7 km from the vent, almost the run-out distance for this current, Figure 6), we can exclude any major control of the PDC run-out distance on the observed temperature variations. On the other hand, an inspection of Figure 6 suggests that a clear relation exists between the measured temperature and the position with respect to the vent, similar to that observed for the EU4 deposits, where differences of at least 30°C have been observed among the deposits from the southern and northern sectors.

[72] Samples from the southern sector (Figure 1a) showing stratified facies indicative of deposition in a turbulent regime from a high-density, stratified current, have high temperatures, ranging from 300 to 360°C. Even higher values (360–380°C) are recorded by massive facies (EU3pf2b) cropping out in the Ercolano excavations. This facies suggests emplacement from a nonturbulent, dense, hot depositional system, completely lacking air ingestion. A basal, fines-poor, ground layer (EU3pf2a_base) emplaced in a turbulent fash-

ion only down flow of obstacles [*Gurioli et al.*, 2002] shows low T_{dep} values (320–340°C), suggesting a cooler frontal portion of the cloud. The high T_{dep} recorded at Ercolano, could have been preserved in this particular location, down current from a significant break in slope of the volcano, which favored the development of a huge depositional fan caused by increases in concentration and deposition rate of the main PDCs [*Gurioli et al.*, 2002].

[73] In summary, the high T_{dep} values of EU3pf deposits recorded in the southern sector, together with their low content of lithic fragments, suggest their deposition from collapse of a hot Plinian fountain with little subsequent air entrainment.

[74] In the northern sector, both the stratified facies on the ridge (Pollena site) and the massive facies confined in the channels (Traianello site) have very similar, low T_{dep} values, ranging from 260°C to 310°C. These low temperatures can be interpreted as due to the presence of the caldera wall of the Somma Vesuvius which favored air entrainment and probably forced an early deposition from the current, reducing the total load and so decreasing its thermal energy. At the Pollena site in a normally graded, stratified deposit, samples from the base record higher temperatures than those collected at the top, in agreement with the emplacement of a stratified current having a normal temperature gradient.

6.4. Type 4 (Very Thick, Massive, Valley-Ponded PDC Deposits)

[75] Type 4 deposits were emplaced en masse by nonturbulent, dense PDCs (Table 1). Their deposits are characterized by a very large fraction of lithic fragments and were generally collected at sites down valley from the caldera rim. The depositional features of these deposits suggest a very minor role of air incorporation in the depositing currents, which rapidly developed a dense underflow.

[76] Despite their high lithic content and their apparent derivation from phreatomagmatic activity, the temperature range estimated for these deposits is not very different from that recorded at the same sites in the deposits of other types of PDCs (Table 2 and Figures 3 and 6). Two possible explanations can be proposed to explain the measured temperatures: (1) that most of the lithics represent preheated fragments because of their provenance from the deeper portions of the magma system and (2) that these PDCs were initially hot and did not undergo important cooling due to water vaporization or air incorporation during transport. Unfortunately, it is practically impossible to fully discriminate between these two possibilities.

[77] EU3pfL and EU8L are rich in lithic fragments of unaltered lava eroded from the first 2000 m of subsurface lithology (Table 1). These lithic fragments were probably warm, but not sufficiently hot to explain the high measured temperature. The deposits of these two units were emplaced en masse from slow moving dense PDCs directly overflowing from the vent, or collapsed from very low, dense fountains. Thus for these units we suggest that the measured temperature reflects rapid, heat preserving, en masse deposition. Furthermore, for these lithic-rich deposits the obstacle represented by the presence of the Somma caldera rim could have contributed to an early unloading of the coarser and heavier lithic blocks already segregated in the basal underflow, so depleting the PDC of its colder material.

[78] Temperature data from type 4 deposits are characterized by a very large scatter at the scale of samples collected at a same site (Table 3). This scatter is practically absent in the other deposits, and probably reflects the occurrence of important thermal inhomogeneities at the scale of the deposit. These could result from the thermal inertia of the abundant boulder-sized lithic fragments of different initial temperature which characterize these deposits.

[79] The phreatomagmatic character attributed to some of these deposits (EU6, EU8L) is not reflected by the relatively high temperatures shown in Table 3. However, although they are stratigraphically related to the accretionary lapilli-bearing depositional sequences dispersed in the southern sector [*Sheridan et al.*, 1981; *Sigurdsson et al.*, 1985; *Cioni et al.*, 1992b], these deposits are characterized by coarse grain sizes and a total absence of macroscopic evidences of important magma-water interaction (accretionary lapilli, mud vesicles, soft sediment deformations). This suggests that magma-water interaction had probably only a minor role in their generation.

7. General Comments

[80] The TRM data on the A.D. 79 PDC deposits can also be used to make some general comments regarding the relationship between the temperature of the deposits and the main physical parameters of the related PDC, as deduced from the sedimentological features of the deposits. The study of a natural case does not allow an unequivocal ''parametrical'' analysis of the various parameters which control the temperature of the deposits, because of their complex interplay. However, the study of the whole sequence of different PDC deposits related to a single eruption allows a better control of some parameters (initial temperature, main features of the juvenile and lithic material, topographical effects on the PDCs).

[81] Notwithstanding the contrasting sedimentological features of the A.D. 79 deposits, temperatures cluster around a value of ~300°C. Temperatures higher than 400°C are rare. A similar result was obtained by *McClelland and Thomas* [1993] on the deposits of the Minoan eruption of Santorini, and could reflect a strong initial temperature decrease of the pyroclastic mixture during the generation of the PDC. This should be borne in mind when discussing the results of the numerical models on PDC transport.

[82] Air incorporation has a major role in controlling the temperature of the deposits. However, in the case of small to medium-scale PDCs (such as those related to the A.D. 79 Vesuvius eruption), air incorporation has a primary role especially in the presence of topographic obstacles, because of local enhancement of turbulence.

[83] On average, samples collected from the Ercolano excavations yield temperatures higher than those from the corresponding units at other sites. The causes of this are not clear. A tentative explanation may be the presence of a very large amount of ignitible material [*Sigurdsson et al.*, 1985] from the town buried and incorporated by the hot deposits, which locally increased the thermal energy and further decreased the cooling rate of the deposits. Even if this hypothesis needs to be corroborated by new data, we should be aware of the bias of the temperature value derived from

deposits which have incorporated large amounts of vegetable remains or wood.

8. Conclusions

[84] The estimated temperatures of the A.D. 79 PDC deposits range from 180 to 380°C, although most of the samples have temperatures between 240 and 340°C. This temperature variation is observed both among the deposits of the same eruptive unit sampled at different sites, and deposits derived by PDCs with similar physical characteristics. The paleomagnetic data, coupled with the sedimentological and stratigraphical picture of the eruption, allow us to draw some important conclusions regarding the physical parameters governing PDC transport and sedimentation, and on the general significance of TRM data on PDC deposits.

[85] First, general considerations suggest that the TRM data for the PDC deposits record the temperature of the deposit (T_{dep}) and not the emplacement temperature.

[86] Second, the main parameters that control the variability of temperature are air ingestion (occurring at the top of the gas thrust region, in the collapsing fountain, and during the flow of the current), involvement of external water and transport and emplacement processes (dilute versus dense, turbulent versus laminar) of the PDCs.

[87] Third, the high lithic clast content of some of these deposits apparently did not play a major role in decreasing the final temperature of the current. This is contrary to the model proposed by *Marti et al.* [1991] because of the medium to fine grain size of the most of these fragments.

[88] Finally, the studied phreatomagmatic deposits show the strong influence of external water in decreasing the temperature of the PDC or creating important temperature inhomogeneities at the scale of a single unit.

[89] **Acknowledgments.** This research was supported by the Italian National Research Council (CNR), Gruppo Nazionale per la Vulcanologia (GNV), the National project INGV-GNV coordinated by Roberto Santacroce, and the University of Torino. Christian Bertagna and Massimo Lanfranco participated in collecting samples and Augusto Neri commented on a preliminary version of the paper. We gratefully acknowledge the reviews by Elizabeth McClelland and two anonymous referees, which enabled us to greatly improve the manuscript. Thanks also to Kathy Cashman, Andy Harris, and Scott Rowland for checking the English.

References

Aramaki, S., and S. Akimoto (1957), Temperature estimation of pyroclastic deposits by natural remanent magnetism, *Am. J. Sci.*, *255*, 619–627.

Barberi, F., H. Bizouard, R. Clocchiatti, N. Metrich, R. Santacroce, and A. Sbrana (1981), The Somma-Vesuvius magma chamber: A petrological and volcanological approach, *Bull. Volcanol.*, *44*, 295–315.

Barberi, F., R. Cioni, M. Rosi, R. Santacroce, A. Sbrana, and R. Vecci (1989), Magmatic and phreatomagmatic phases in explosive eruptions of Vesuvius as deduced by grain-size and compositional analysis of pyroclastic deposits, *J. Volcanol. Geotherm. Res.*, *38*, 287–307.

Bardot, L. (2000), Emplacement temperature determinations of proximal pyroclastic deposits on Santorini, Greece, and their implications, *Bull. Volcanol.*, *61*, 450–467.

Bardot, L., and E. McClelland (2000), The reliability of emplacement temperature estimates using palaeomagnetic methods: A case study from Santorini, Greece, *Geophys. J. Int.*, *143*(1), 39–51.

Basile, C. (1994), I papiri carbonizzati di Ercolano, quaderni, 93 pp., Assoc. Ist. Int. del Papiro, Siracusa, Italy.

Burgisser, A., and G. W. Bergantz (2002), Reconciling pyroclastic flow and surge: The multiphase physic of pyroclastic density currents, *Earth Planet. Sci. Lett.*, *202*, 405–418.

Bursik, M. I., and A. W. Woods (1996), The dynamics and thermodynamics of large ash flows, *Bull. Volcanol.*, *58*, 175–193.

Butler, R. F. (1992), *Paleomagnetism*, 319 pp., Blackwell Sci., Malden, Mass.

Carlsaw, H. S., and J. C. Jaeger (1959), *Conduction of Heat in Solids*, 510 pp., Oxford Univ. Press, New York.

Cioni, R., A. Sbrana, and R. Vecci (1992a), Morphological features of juvenile pyroclasts from magmatic to phreatomagmatic deposits of Vesuvius, *J. Volcanol. Geotherm. Res.*, *51*, 61–78.

Cioni, R., P. Marianelli, and A. Sbrana (1992b), Dynamics of the AD 79 eruption: Stratigraphic, sedimentological and geochemical data on the successions of the Somma-Vesuvius southern and eastern sectors, *Acta Vulcanol.*, *2*, 109–123.

Cioni, R., L. Civetta, P. Marianelli, N. Metrich, R. Santacroce, and A. Sbrana (1995), Compositional layering and syneruptive mixing of a periodically refilled shallow magma chamber: The AD 79 Plinian eruption of Vesuvius, *J. Petrol.*, *36*(3), 739–776.

Cioni, R., A. Sbrana, and L. Gurioli (1996), The deposits of AD 79 eruption, in *Vesuvius decade Volcano Workshop Handbook*, edited by R. Santacroce et al., pp. E1–E31, Cons. Nac. Ric., Rome, Italy.

Cioni, R., R. Santacroce, and A. Sbrana (1999), Pyroclastic deposits as a guide for reconstructing the multi-stage evolution of the Somma-Vesuvius Caldera, *Bull. Volcanol.*, *60*, 207–222.

Clement, B. M., C. B. Connor, and G. Graper (1993), Paleomagnetic estimate of the emplacement temperature of the long-runout Nevado de Colima volcanic debris avalanche deposit, Mexico, *Earth Planet. Sci. Lett.*, *120*, 499–510.

Dobran, F., and P. Papale (1993), Magma-water interaction in closed systems and application to lava tunnels and volcanic conduits, *J. Geophys. Res.*, *98*, 14,041–14,058.

Dobran, F., A. Neri, and G. Macedonio (1993), Numerical simulation of collapsing volcanic columns, *J. Geophys. Res.*, *98*, 4231–4259.

Downey, W. S., and D. H. Tarling (1991), Reworking characteristics of Quaternary pyroclastics, Thera (Greece), determined using magnetic properties, *J. Volcanol. Geotherm. Res.*, *46*, 143–155.

Druitt, T. H. (1998), Pyroclastic density current, in *The Physics of Explosive Volcanic Eruptions*, edited by J. S. Gilbert and R. S. J. Sparks, *Geol. Soc. Spec. Publ.*, *145*, 145–182.

Evans, M. E., and M. Mareschal (1986), An archeomagnetic example of polyphase magnetization, *J. Geomagn. Geoelectr.*, *38*, 923–929.

Freundt, A., and M. I. Bursik (1998), Pyroclastic flow transport mechanism, in *From Magma to Tephra: Modelling Physical Processes of Explosive Volcanic Eruptions*, edited by A. Freundt and M. Rosi, pp. 173–246, Elsevier Sci., New York.

Gurioli, L. (2000), Pyroclastic flow: Classification, transport and emplacement mechanisms, *Plinius*, *23*, 84–89.

Gurioli, L., R. Cioni, and C. Bertagna (1999), I depositi di flusso piroclastico dell'eruzione del 79 d. C.: Caratterizzazione stratigrafica, sedimentologica e modelli di trasporto e deposizione, *Atti Soc. Tosc. Sci. Nat. Mem., Ser. A*, *106*, 61–72.

Gurioli, L., R. Cioni, A. Sbrana, and E. Zanella (2002), Transport and deposition from pyroclastic flows over densely inhabited areas: Ercolano (Italy), *Sedimentology*, *46*, 1–26.

Hoblitt, R. P., and K. S. Kellogg (1979), Emplacement temperature of unsorted and unstratified deposits of volcanic debris as determined by palaeomagnetic techniques, *Geol. Soc. Am. Bull.*, *90*, 633–642.

Inman, D. L. (1952), Measures for describing the size distribution of sediments, *J. Sediment. Petrol.*, *22*, 125–145.

Jaeger, J. C. (1968), Cooling and solidification of igneous rocks, in *Basalts*, vol. 2, edited by H. H. Hess and A. Poldevaart, pp. 503–536, Wiley-Interscience, Hoboken, N. J.

Kent, D. V., D. Ninkovich, T. Pescatore, and R. S. J. Sparks (1981), Palaeomagnetic determination of emplacement temperature of Vesuvius AD 79 pyroclastic deposits, *Nature*, *290*, 393–396.

Koyaguchi, T., and A.W. Woods (1996), On the formation of eruption columns following explosive mixing of magma and surface-water, *J. Geophys. Res.*, *101*, 5561–5574.

Kozu, S. (1934), The great activity of Komagatake in 1929, *Mineral. Petrogr. Mitt.*, *45*, 133–174.

Mandeville, C. W., S. Carey, H. Sigurdsson, and J. King (1994), Paleomagnetic evidence for high-temperature emplacement of the 1883 subaqueous pyroclastic flows from Krakatau Volcano, Indonesia, *J. Geophys. Res.*, *99*, 9487–9504.

Marti, J., J. L. Diez-Gil, and R. Ortiz (1991), Conduction model for the thermal influence of lithic clasts in mixtures of hot gases and ejecta, *J. Geophys. Res.*, *96*, 21,879–21,885.

Marton, P., D. H. Tarling, G. Nardi, and D. Pierattini (1993), An archaeomagnetic study of roof tiles from temple E. Selinunte, Sicily, *Sci. Technol. Cult. Heritage*, *2*, 131–136.

Mastrolorenzo, G., P. P. Petrone, M. Pagano, A. Incoronato, P. J. Baxter, A. Canzanella, and L. Fattore (2001), Herculaneum victims of Vesuvius in AD 79, *Nature*, *410*, 769–770.

McClelland-Brown, E. (1982), Discrimination of TRM and CRM by blocking temperature spectrum analysis, *Phys. Earth Planet. Inter.*, *30*, 404–414.

McClelland, E. A., and T. H. Druitt (1989), Palaeomagnetic estimates of emplacement temperatures of pyroclastic deposits on Santorini, Greece, *Bull. Volcanol.*, *51*, 16–27.

McClelland, E., and R. Thomas (1993), A palaeomagnetic study of Minoan age tephra from Thera, in *Thera and the Aegean World III*, vol. 2, edited by D. Hardy, pp. 129–138, Thera Found., London.

Miller, T. F. (1990), A numerical model of volatile behavior in nonwelded cooling pyroclastic deposits, *J. Geophys. Res.*, *95*, 19,349–19,364.

Pullaiah, G., E. Irving, K. L. Buchan, and D. J. Dunlop (1975), Magnetization changes caused by burial and uplift, *Earth Planet. Sci. Lett.*, *28*, 133–143.

Riehle, J. R., T. F. Miller, and R. A. Bailey (1995), Cooling, degassing and compaction of rhyolitic ash flow tuffs: Computational model, *Bull. Volcanol.*, *57*, 319–336.

Ryan, M. P., N. G. Banks, R. P. Hoblitt, and J. Y. K. Blevins (1990), The in-situ transport properties and the thermal structure of Mount St Helens eruptive units, in *Magma Transport and Storage*, edited by M. P. Ryan, pp. 137–155, John Wiley, Hoboken, N. J.

Sheridan, M. F., F. Barberi, M. Rosi, and R. Santacroce (1981), A model for Plinian eruptions of Vesuvius, *Nature*, *289*, 282–285.

Sigurdsson, H., S. Cashdollar, and R. S. J. Sparks (1982), The eruption of Vesuvius in AD 79: Reconstruction from historical and volcanological evidence, *Am. J. Archaeol.*, *86*, 39–51.

Sigurdsson, H., S. Carey, W. Cornell, and T. Pescatore (1985), The eruption of Vesuvius in 79 AD, *Nat. Geogr. Res.*, *1*, 332–387.

Sparks, R. S. J. (1976), Variations in ignimbrites and implications for the transport of pyroclastic flows, *Sedimentology*, *23*, 147–188.

Sparks, R. S. J., M. I. Bursik, S. N. Carey, J. S. Gilbert, L. S. Glaze, H. Sigurdsson, and A. W. Woods (1997), *Volcanic Plumes*, 574 pp., John Wiley, Hoboken, N. J.

Tanguy, J. C., M. Le-Goff, V. Chillemi, A. Paiotti, C. Principe, S. L. Delfa, and G. Patane (1999), Secular variation in geomagnetic field direction recorded in lavas from Etna and Vesuvius during the last two millennia, *C. R. Acad. Sci., Ser. II*, *329*(8), 557–564.

Todesco, M., A. Neri, T. Esposti Onagro, P. Papale, G. Macedonio, R. Santacroce, and A. Longo (2002), Pyroclastic flow hazard assessment at Vesuvius (Italy) by using numerical modeling. I. Large-scale dynamics, *Bull. Volcanol.*, *64*, 155–177.

Valentine, G. A. (1987), Stratified flow in pyroclastic surges, *Bull. Volcanol.*, *49*, 616–630.

Varekamp, J. C. (1993), Some remarks on volcanic vent evolution during plinian eruptions, *J. Volcanol. Geotherm. Res.*, *54*, 309–318.

Vecci, R. (1992), L'interazione esplosiva magma/acqua: Caratterizzazione dei prodotti e meccanismi eruttivi, Ph.D. thesis, 388 pp., Univ. of Pisa, Pisa, Italy.

Wright, J. V. (1978), Remanent magnetism of poorly sorted deposits from the Minoan eruption of Santorini, *Bull. Volcanol.*, *41*, 131–135.

Zanella, E., L. Gurioli, G. Chiari, A. Ciarallo, R. Cioni, E. De Carolis, and R. Lanza (2000), Archaeomagnetic results from mural paintings and pyroclastic rocks in Pompeii and Herculaneum, *Phys. Earth. Planet. Inter.*, *118*, 227–240.

Zijderveld, J. D. A. (1967), Analysis of results, in *Methods in Palaeomagnetism*, edited by D. W. Collinson, K. M. Creer, and S. K. Runcorn, pp. 254–286, Elsevier Sci., New York.

R. Cioni, Dipartimento di Scienze della Terra, Via Trentino 51, 09127, Cagliari, Italy. (rcioni@unica.it)

L. Gurioli, Istituto di Geoscienze e Georisorse, CNR, Via Morruzzi, 1, I-56126, Pisa, Italy. (gurioli@igg.cnr.it)

R. Lanza and E. Zanella, Dipartimento di Scienze della Terra, Via Valperga Caluso 35, 10125, Torino, Italy. (roberto.lanza@unito.it; elena.zanella@unito.it)